

## Measurement of $J/\psi$ production cross-section in pp collisions at $\sqrt{s} = 13$ TeV at LHCb

---

**Komarov Ilya\*** on behalf of LHCb collaboration

*Ecole Polytechnique Fédérale de Lausanne (CH)*

*E-mail: [ila.komarov@cern.ch](mailto:ila.komarov@cern.ch)*

The production of  $J/\psi$  mesons in proton-proton collisions at a center-of-mass energy of  $\sqrt{s} = 13$  TeV is studied with the LHCb detector. Cross-section measurements are performed as a function of the transverse momentum  $p_T$  and the rapidity  $y$  of the  $J/\psi$  meson in the region  $p_T < 14$  GeV/ $c$  and  $2.0 < y < 4.5$ , for both prompt  $J/\psi$  mesons and  $J/\psi$  mesons from  $b$ -hadron decays. The production cross-sections integrated over the kinematic coverage are  $15.30 \pm 0.03 \pm 0.86$   $\mu\text{b}$  for prompt  $J/\psi$  and  $2.34 \pm 0.01 \pm 0.13$   $\mu\text{b}$  for  $J/\psi$  from  $b$ -hadron decays, assuming zero polarization of the  $J/\psi$  meson. The first uncertainties are statistical and the second systematic. The ratios of the cross-sections with respect to  $\sqrt{s} = 8$  TeV are also determined.

*The European Physical Society Conference on High Energy Physics  
22–29 July 2015  
Vienna, Austria*

---

\*Speaker.

## 1. Introduction

Heavy quarkonium in  $pp$  collisions is produced in two stages. The first stage is the production of a heavy  $Q\bar{Q}$  pair and this process is well-described perturbatively. At the second stage, the heavy  $Q\bar{Q}$  pair hadronizes to a quarkonium state. Two main approaches to the description of the  $J/\psi$  production are the color-singlet model (CSM) [1] and the non-relativistic QCD (NRQCD) [2]. The color singlet model assumes the intermediate  $Q\bar{Q}$  state to be colorless, whereas NRQCD allows it to have all allowed quantum numbers. NRQCD calculations require experimental inputs, namely the long-distance matrix elements (LDME) [3] to calculate the probability of the transformation of a  $Q\bar{Q}$  state with the specific configuration of quantum numbers to the final quarkonium state. Both NRQCD and CSM predictions are in agreement with previous cross-section measurements [4–6], but they give contradictory estimations of the  $J/\psi$  polarization at high transverse momentum,  $p_T$ , [7] which are not confirmed by experimental results [8].

Together with  $J/\psi$  mesons produced directly in hard collisions of partons or through the feed-down of excited quarkonium states, which are referred in this text as prompt  $J/\psi$ , high energy  $pp$  collisions also produce  $J/\psi$  mesons as the decay products of  $b$ -hadrons. In this document such mesons are referred to as “ $J/\psi$ -from- $b$ ”. The production cross-section of  $J/\psi$ -from- $b$  and its dependence on  $p_T$  are described with the Fixed Order plus Next-to-Leading Logarithms (FONLL) formalism [9].

Under the assumption of zero  $J/\psi$  polarization, the following quantities are measured: the double differential cross-sections of prompt  $J/\psi$  and  $J/\psi$ -from- $b$  as function of  $p_T$  and  $y$ ; the integrated production cross-sections for prompt  $J/\psi$  and  $J/\psi$ -from- $b$ ; the  $b\bar{b}$  production cross-section; and the ratio of the cross-sections with respect to the  $J/\psi$  cross-sections in  $pp$  collisions at  $\sqrt{s} = 8$  TeV previously measured by the LHCb [10].

This paper is an abridged version of Ref. [11] by the LHCb collaboration, which contains a full description of the analysis.

## 2. New trigger scheme

This analysis benefits from a new scheme for the LHCb software trigger introduced for LHC Run 2. The alignment and the calibration are performed in nearly real-time [12] and updated alignment constants are made available for the trigger. The same alignment and calibration information is propagated to the offline reconstruction, to ensure consistent and high-quality particle identification information for the trigger and offline reconstruction. The larger time budget available in the trigger with respect to the LHCb Run 1 also results in the convergence of the online and offline track reconstructions, such that the offline performance is achieved in the trigger. The identical performance of the online and offline reconstruction achieved in this way offers the opportunity to perform physics analyses directly using candidates reconstructed in the trigger [13]. The storage of only the triggered candidates enables a reduction in the event size by an order of magnitude. The analysis described in this document uses the online reconstruction for the first time in LHCb, and is checked against the standard offline reconstruction chain.

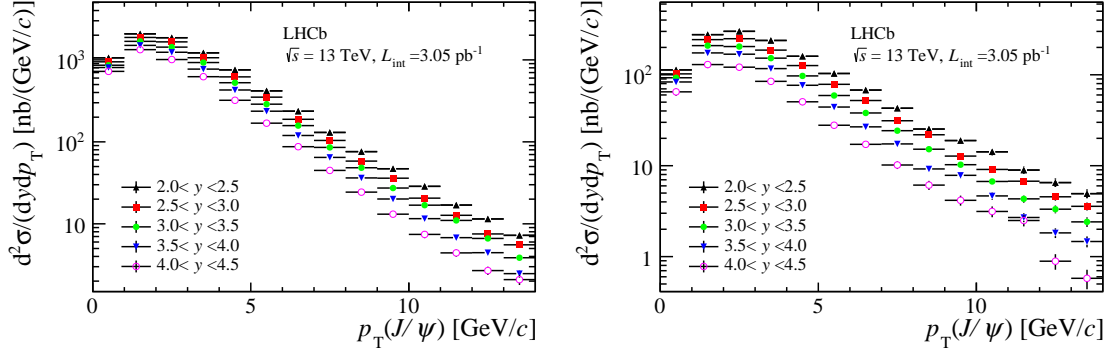


Figure 1: Double differential cross-sections for prompt  $J/\psi$  (left) and  $J/\psi$ -from- $b$  (right) mesons as functions of  $p_T$  in bins of  $y$ . Statistical and systematic uncertainties are added in quadrature.

### 39 3. Cross-section determination

40 The data used in this analysis come from  $pp$  collisions at  $\sqrt{s} = 13$  TeV, collected by the LHCb  
 41 detector [14] in July 2015, with an average of 1.1 visible interactions per bunch crossing and  
 42 corresponding to an integrated luminosity of  $3.05 \pm 0.12 \text{ pb}^{-1}$ .

43 The online event selection consists of a hardware stage, based on information from the calorime-  
 44 ter and muon systems, followed by a software stage, which performs the  $J/\psi$  candidate reconstruc-  
 45 tion. In this analysis the  $J/\psi$  candidates are reconstructed from the two opposite-charged muons.  
 46 The main selection criteria are based on the kinematics of the muons and on the quality of the  
 47 primary vertex (PV) and the two-track vertex of the  $J/\psi$  candidate.

48 The double differential  $J/\psi$  production cross-section in each kinematic bin of  $p_T$  and  $y$  is  
 49 defined as

$$\frac{d^2\sigma}{dy dp_T} = \frac{N(J/\psi \rightarrow \mu^+\mu^-)}{L_{\text{int}} \times \epsilon_{\text{tot}} \times \mathcal{B}(J/\psi \rightarrow \mu^+\mu^-) \times \Delta y \times \Delta p_T}, \quad (3.1)$$

50 where  $N(J/\psi \rightarrow \mu^+\mu^-)$  is the yield of prompt  $J/\psi$  or  $J/\psi$ -from- $b$  signals in the given kinematic  
 51 bin,  $\epsilon_{\text{tot}}$  is the total detection efficiency in the given kinematic bin,  $L_{\text{int}}$  is the integrated luminosity,  
 52  $\mathcal{B}(J/\psi \rightarrow \mu^+\mu^-) = (5.961 \pm 0.033)\%$  [15] is the branching ratio of the decay  $J/\psi \rightarrow \mu^+\mu^-$  and  
 53  $\Delta p_T = 1 \text{ GeV}/c$  and  $\Delta y = 0.5$  are the bin widths. The yield of  $J/\psi$  signal events, both from prompt  
 54  $J/\psi$  and  $J/\psi$ -from- $b$ , is determined from a two-dimensional unbinned maximum likelihood fit to the  
 55 invariant mass and pseudo proper time of the candidates, performed independently for each  $(p_T, y)$   
 56 bin. The pseudo proper time is defined as

$$t_z = \frac{(z_{J/\psi} - z_{\text{PV}}) \times M_{J/\psi}}{p_z}, \quad (3.2)$$

57 where  $z_{J/\psi} - z_{\text{PV}}$  is the difference of the positions along the beam axis between the  $J/\psi$  decay vertex  
 58 and the PV,  $p_z$  is the  $z$ -component of the  $J/\psi$  momentum, and  $M_{J/\psi}$  the known  $J/\psi$  mass [15]. The  
 59 reconstructed vertex of the  $J/\psi$  meson originating from  $b$ -hadron decays tends to be separated from  
 60 the PVs, and thus it can be distinguished from prompt  $J/\psi$  mesons from the fit to the pseudo proper  
 61 time.

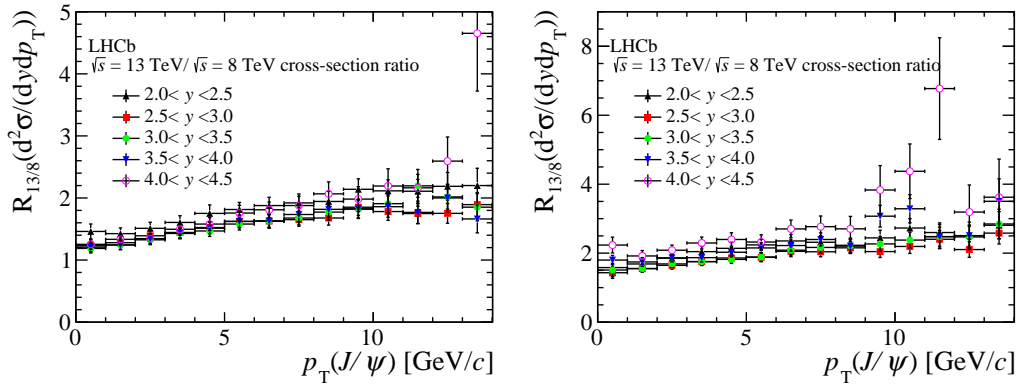


Figure 2: Ratios of differential cross-sections between measurements at  $\sqrt{s} = 13$  TeV and  $\sqrt{s} = 8$  TeV as functions of  $p_T$  in bins of  $y$  for (left) prompt  $J/\psi$  mesons and (right)  $J/\psi$ -from- $b$  mesons.

## 62 4. Results

63 The measured double differential cross-sections for prompt  $J/\psi$  and  $J/\psi$ -from- $b$  mesons,  
 64 assuming no polarization, are shown in Fig. 1, whereas the cross-sections integrated over all ( $p_T, y$ )  
 65 bins in the kinematic range  $p_T < 14$  GeV/ $c$  and  $2.0 < y < 4.5$  are:

$$\begin{aligned} \sigma(\text{prompt } J/\psi, p_T < 14 \text{ GeV}/c, 2.0 < y < 4.5) &= 15.30 \pm 0.03 \pm 0.86 \mu\text{b}, \\ \sigma(J/\psi\text{-from-}b, p_T < 14 \text{ GeV}/c, 2.0 < y < 4.5) &= 2.34 \pm 0.01 \pm 0.13 \mu\text{b}, \end{aligned}$$

66 where the first uncertainties are statistical and the second systematic.

67 In addition to absolute values, the double differential production cross-sections of prompt and  
 68  $J/\psi$ -from- $b$  mesons in  $pp$  collisions at the center-of-mass energy of  $\sqrt{s} = 13$  TeV were measured  
 69 relatively to that of  $\sqrt{s} = 8$  TeV ( $R_{13/8}$ ) and are presented in Fig. 2.

70 The calculation of the ratio of the two measurements allows to reduce some correlated un-  
 71 certainties. In particular, significant improvement was achieved for the systematical uncertainty  
 72 coming from the luminosity, the tracking and trigger efficiencies. Some of the uncertainties in the  
 73 theoretical predictions were also canceled. For example, the leading uncertainty of the NRQCD  
 74 prediction, caused by LDME, canceled almost completely and no theoretical uncertainty is given for  
 75 this prediction.

76 The calculation of the ratio also allows to improve the FONLL predictions. Since the scale  
 77 choice made at the two energies (8 TeV and 13 TeV) is correlated, uncertainties of this type are  
 78 partially canceled. Other parameters such as the heavy quark mass, the fragmentation fractions  
 79 to specific hadrons, the fragmentation functions and the decay branching ratios are also fully  
 80 correlated at different energies and lead to negligible systematic uncertainties in the cross-section  
 81 ratios [16]. Thus, the main sources of the remaining uncertainty of FONLL predictions for the  
 82 cross-section ratios are the scale dependence, the choice of the heavy quark mass and the parton  
 83 distribution functions (PDF). The cancelation of correlated theoretical uncertainties makes it possible  
 84 to distinguish the predictions based on different PDFs, which leads to possibly useful constraints on  
 85 parton density functions.

86 The measured ratios of the differential production cross-section as functions of  $p_T$  and  $y$ ,  
 87 together with available theoretical predictions are presented in Fig. 3.

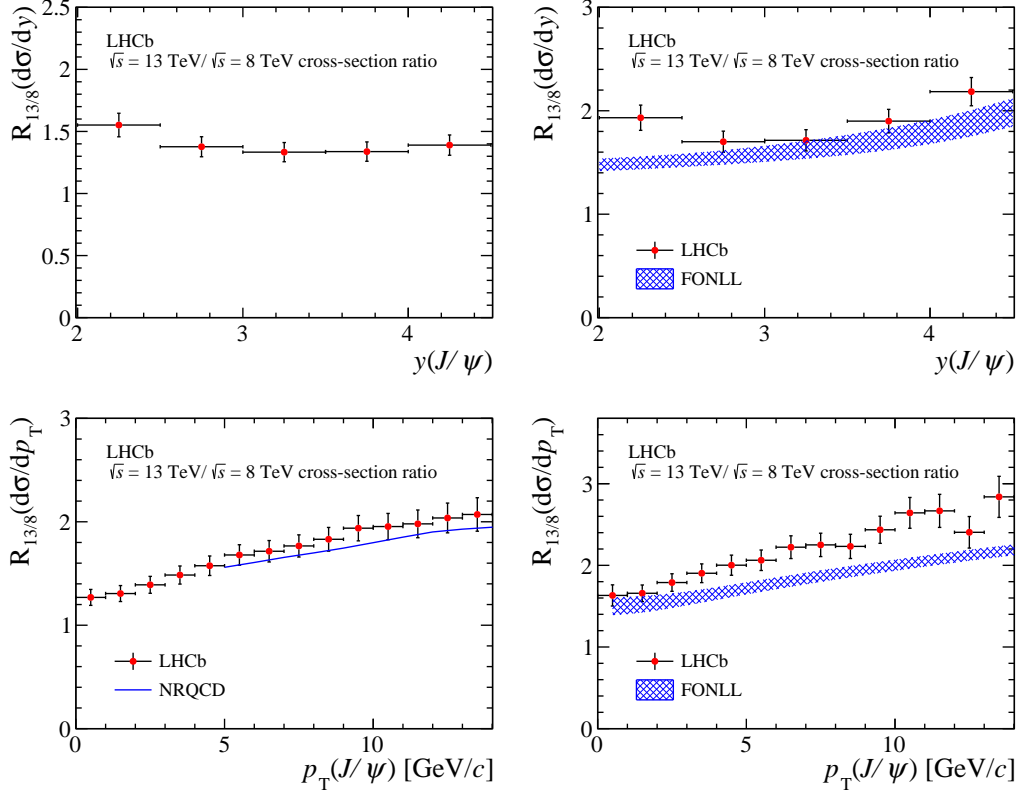


Figure 3: Ratios of differential cross-sections between measurements at  $\sqrt{s} = 13$  TeV and  $\sqrt{s} = 8$  TeV as functions of  $y$  integrated over  $p_T$  (top row) and as functions of  $p_T$  integrated over  $y$  (bottom row) for prompt  $J/\psi$  (left column) and  $J/\psi$ -from- $b$  mesons (right column). Calculations of NRQCD [17] and FONLL [16] are compared to prompt  $J/\psi$  mesons and  $J/\psi$ -from- $b$  mesons, respectively.

## 88 5. Conclusions

89 A new LHCb trigger scheme is used for the first time to collect data for this analysis. These data  
 90 allowed to measure the differential  $J/\psi$  production cross-sections in  $pp$  collisions at a center-of-mass  
 91 energy of  $\sqrt{s} = 13$  TeV for prompt and  $J/\psi$ -from- $b$  mesons and the ratios to those at  $\sqrt{s} = 8$  TeV in  
 92 bins of transverse momentum and rapidity in the range of  $p_T < 14$  GeV/c and  $2.0 < y < 4.5$ . The  
 93 calculation of a ratio of the production cross-sections allowed to decrease the uncertainties both for  
 94 the measures and the predicted values, which leads to a more stringent test of the theory.

95 The theoretical predictions based on NRQCD accurately describe the  $p_T$  dependence of the  
 96 ratio of the production cross-section measurements at  $\sqrt{s} = 13$  TeV and  $\sqrt{s} = 8$  TeV for a prompt  
 97  $J/\psi$  mesons. The theoretical prediction based on FONLL undershoot the  $p_T$  dependence of the  
 98 ratio for  $J/\psi$ -from- $b$ , but is in agreement with the rapidity dependence of the ratio for the production  
 99 cross-section measurements at  $\sqrt{s} = 13$  TeV and  $\sqrt{s} = 8$  TeV.

100 **References**

- 101 [1] R. Baier and R. Rückl, *Hadronic production of  $J/\psi$  and  $\Upsilon$ : Transverse momentum distributions*, *Phys.*  
102 *Lett.* **B102** (1981) 364.
- 103 [2] G. T. Bodwin, E. Braaten, and G. P. Lepage, *Rigorous QCD analysis of inclusive annihilation and*  
104 *production of heavy quarkonium*, *Phys. Rev.* **D51** (1995) 1125, [arXiv:hep-ph/9407339](#).
- 105 [3] J. P. Lansberg,  *$J/\psi$ ,  $\psi'$  and  $\Upsilon$  production at hadron colliders: A Review*, *Int. J. Mod. Phys.* **A21** (2006)  
106 3857, [arXiv:hep-ph/0602091](#).
- 107 [4] M. Cacciari, M. Greco, M. L. Mangano, and A. Petrelli, *Charmonium production at the Tevatron*, *Phys.*  
108 *Lett.* **B356** (1995) 553, [arXiv:hep-ph/9505379](#).
- 109 [5] Y.-Q. Ma, K. Wang, and K.-T. Chao, *Complete next-to-leading order calculation of the  $J/\psi$  and  $\psi'$*   
110 *production at hadron colliders*, *Phys. Rev.* **D84** (2011) 114001, [arXiv:1012.1030](#).
- 111 [6] J. P. Lansberg,  *$J/\psi$  production at  $\sqrt{s}=1.96$  and 7 TeV: Color-Singlet Model, NNLO\* and polarisation*,  
112 *J. Phys.* **G38** (2011) 124110, [arXiv:1107.0292](#).
- 113 [7] M. Butenschoen and B. A. Kniehl,  *$J/\psi$  polarization at Tevatron and LHC: Nonrelativistic-QCD*  
114 *factorization at the crossroads*, *Phys. Rev. Lett.* **108** (2012) 172002, [arXiv:1201.1872](#).
- 115 [8] LHCb, R. Aaij *et al.*, *Measurement of  $J/\psi$  polarization in  $pp$  collisions at  $\sqrt{s} = 7$  TeV*, *Eur. Phys. J.*  
116 **C73** (2013), no.~11 2631, [arXiv:1307.6379](#).
- 117 [9] M. Cacciari, M. Greco, and P. Nason, *The  $p_T$  spectrum in heavy flavor hadroproduction*, *JHEP* **05**  
118 (1998) 007, [arXiv:hep-ph/9803400](#).
- 119 [10] LHCb collaboration, R. Aaij *et al.*, *Production of  $J/\psi$  and  $\Upsilon$  mesons in  $pp$  collisions at  $\sqrt{s} = 8$  TeV*,  
120 *JHEP* **06** (2013) 064, [arXiv:1304.6977](#).
- 121 [11] LHCb, R. Aaij *et al.*, *Measurement of forward  $J/\psi$  production cross-sections in  $pp$  collisions at*  
122  *$\sqrt{s} = 13$  TeV*, [arXiv:1509.00771](#).
- 123 [12] G. Dujany and B. Storaci, *Real-time alignment and calibration of the LHCb Detector in Run II*,  
124 [LHCb-PROC-2015-011](#).
- 125 [13] R. Aaij *et al.*, *The LHCb trigger and its performance in 2011*, *JINST* **8** (2013) P04022,  
126 [arXiv:1211.3055](#).
- 127 [14] LHCb collaboration, A. A. Alves Jr. *et al.*, *The LHCb detector at the LHC*, *JINST* **3** (2008) S08005.
- 128 [15] Particle Data Group, K. A. Olive *et al.*, *Review of particle physics*, *Chin. Phys.* **C38** (2014) 090001.
- 129 [16] M. Cacciari, M. L. Mangano, and P. Nason, *Gluon PDF constraints from the ratio of forward heavy*  
130 *quark production at the LHC at  $\sqrt{s} = 7$  and 13 TeV*, [arXiv:1507.06197](#).
- 131 [17] H.-S. Shao *et al.*, *Yields and polarizations of prompt  $J/\psi$  and  $\psi(2S)$  production in hadronic collisions*,  
132 *JHEP* **05** (2015) 103, [arXiv:1411.3300](#).